

# Dynamical friction for dark halo satellites: effects of tidal massloss and growing host potential

HongSheng Zhao<sup>1</sup>

*University of St. Andrews, Physics and Astronomy, KY16 9SS, Scotland<sup>2</sup>*

*Institute of Astronomy, Cambridge, CB30HA, England*

## ABSTRACT

Motivated by observations of inner halo satellite remnants like the Sgr and  $\omega$ -Centauri, we develop fully analytical models to study the orbital decay and tidal massloss of satellites on eccentric orbits in an isothermal potential of a host galaxy halo. The orbital decay rate is often severely overestimated if applying the Chandrasekhar's formula without correcting for (a) the evaporation and tidal loss of the satellite and (b) the contraction of satellite orbits due to adiabatic growth of the host galaxy potential over the Hubble time. As a satellite migrates inwards, the increasing halo density affects the dynamical friction in two opposite ways: (1) it boosts the number of halo particles swept in the satellite's gravitational "wake", hence increasing the drag on the satellite, and (2) it boosts the tide which "peels off" the satellite, and reduces the amplitude of the wake. These competing processes can be modeled analytically for a satellite with the help of an empirical formula for the massloss history. The analytical model agrees with more traditional numerical simulations of tidal massloss and dynamical friction. Rapid massloss due to increasing tides at smaller and smaller radius makes it less likely for streams or remnants of infalling satellites to intrude the inner halo (as the Sgr stream and  $\omega$ -Centauri) than to stay in the outer halo (as the Magellanic stream), hence any intermediate-mass central black holes of the satellites are also likely "hung up" at large distances as well. It is difficult for the satellites' black holes to come close enough to merge into the supermassive black hole in the center of the host potential unless the satellites started with (i) pericenters much smaller than the typical distances to present-day observed satellites and with (ii) central density much higher than in the often seen finite density cores of observed satellites.

*Subject headings:* Galaxy: halo - Galaxy: kinematics and dynamics - galaxies: dwarf - dark matter - methods: analytical

## 1. Introduction

Current theory of galaxy formation favors the idea that galaxies form hierarchically by merging smaller lumps or satellites. The gravity from a moving satellite pulls behind it a "wake" of particles of the host galaxy (ChandraSekhar 1943, Mulder 1983). This dynamical friction dissipates the orbital energy of the satellites so that they sink deep into the host galaxy potential well, where they are disintegrated and virialized via baryonic feedbacks and tidal stripping. These processes might have determined the density profile of virialized halo of the host galaxy (Syer & White 1998, Dekel et al. 2003).

There are about 150 and 300 globular clusters, and a few dozen dwarf satellites of mass  $10^{6-9}M_{\odot}$  in the Milky Way and M31 respectively. It is tempting to associate these dwarfs satellites and globular clusters as the markers/remnants of past hierarchical merging events. Indeed there are several examples of possible streams of remnants in the Milky Way (Lynden-Bell & Lynden-Bell 1995) including the recently found Galactic ring or Carnis Major dwarf galaxy, traced by a grouping of globular clusters (Martin et al. 2004). A giant stream is found in the Andromeda galaxy (McConnachie et al. 2003, Ferguson et al, 2002). Among these the Sagittarius dwarf galaxy stream (Ibata et al. 1997) between radius 10-50 kpc from the Galactic center is perhaps the best example. It brings in at least 5 globular clusters to the inner halo, including M54, the 2nd most massive cluster of the Milky Way. A still mysterious object is  $\omega$ -Centauri, with about  $10^6L_{\odot}$  at 5 kpc from the Galactic center which has the morphology of a globular cluster, but has multiple epochs of star formation and chemical enrichment (see Gnedin et al. 2002 and the  $\omega$ -Centauri symposium). Another example is the G1 cluster, a very massive globular-like object with about  $10^6L_{\odot}$  at about 40 kpc from the M31 center (Meylan et al. 2001). A system (NGC1023-13) almost identical to G1 is also found in the S0 galaxy NGC1023, at a projected distance of about 40 kpc from the host galaxy (Larsen 2001). Freeman (1993) suggested that such systems are the remnants of nucleated dwarf satellites, with their outer tenuous dark matter and stars being removed by galaxy tides. M31 also has an unusual collection of clusters as luminous as  $\omega$ -Centauri within 5 kpc in projection from its double-peaked center. Given the above evidences or signs for infalling objects in our galaxy and M31, it is interesting to ask whether some of the inner globulars could have also been the result of mergers. Beyond the Local Group, minor mergers are sometimes speculated as the mechanism to deliver massive black holes and gas material into the nucleus of an AGN to account for the directions of the jets and nuclear dusty disks (Kendall, Magorrian, & Pringle 2003). A very interesting related issue is whether giant black

---

<sup>1</sup>UK PPARC Advanced Fellowship and Visiting Professorship at Beijing Observatory

<sup>2</sup>Present address (hz4@st-andrews.ac.uk)

holes acquire part of the mass by merging the smaller black holes in the nuclei of infalling satellites.

For this paper we revisit the basic theoretical questions: what is the condition for a dwarf galaxy to decay into the inner halo? What are the possible outcomes of tidal stripping of a dwarf satellite? How often do we get a system like  $\omega$ -Centauri or a naked black hole near the host center? The answers to these questions will help us to test the validity of the theory of hierarchical merger formation of galaxies. The key mechanism for satellites to enter the inner galaxy is dynamical friction, where the gravity of the satellite creates a wake of overdensities in the particle distribution of the host galaxy, which in turn drags the motion of the satellite with a force proportional to  $m(t)^2$ , where  $m(t)$  is the mass of the satellite. Another process is tidal disruption, where the object sheds mass with each pericenter passage, and the remnants are littered along the orbit of the satellite. The above two processes compete with and regulate each other: orbital decay increases the tidal field, which reduces the mass of the satellite, hence slows down the orbital decay. Some examples of these effects have been shown in Zhao (2002) in the case of  $\omega$ -Centauri .

The analytical formula of Chandrasekhar is widely used for gaining insights on dynamical friction because of the time-consuming nature of the more rigorous N-body numerical simulation approach. It is a customary practice in previous works to model the orbital decay of a satellite as a point mass of a fixed mass. However, *the fixed-mass approximation is invalid* and could seriously overestimate dynamical friction because of neglecting massloss  $\frac{dm(t)}{dt}$ . It is essential in calculations of satellite orbits to model the dynamical friction and massloss together since they regulate each other.

In the past the massloss and the orbital decay are often modeled in the *ab initio* fashion, resulting coupled non-linear equations without simple analytical solutions. In such models, the satellite mass is often modeled as a function of the satellite’s tidal radius, hence various factors come in, including the orbital position of the satellite, the density profile of the satellite (e.g., Jiang & Binney 2000, Zhao 2002, Mouri & Taniguchi 2003, Kendall et al. 2003). However, these complications are not always necessary since the massloss history is rather similar in simulations with very different initial conditions (the mass is generally a stair-case like a function of the time), so could be parametrized in an empirical fashion, by-passing the uncertain assumptions of the satellite initial profile. This could be useful for exploring a large parameter space of the satellite initial condition.

Another invalid approximation but common practice is to use a static potential for the host galaxy. This again is unphysical since galaxy halos do grow in hierarchical formation scenario partly because of galaxy merging, and partly because of the adiabatic contraction of the baryonic disk and bulge; galaxy rotation curves  $V_{\text{cir}}(r, t)$  can change by significantly

before and after the formation of baryonic disks and bulges in mass models for the Milky Way and M31 (Klypin, Zhao & Somerville 2002) and in generic CDM simulations with baryons (e.g. Wright 2003). The growing gravitational force tends to restrain the radial excursions of the satellite while preserving the angular momentum. The dynamical friction or drag force is also proportional to the growing density  $\rho(r, t)$  of ambient stars and dark particles in the host galaxy.

In fact, it is conceptually simple to incorporate massloss and growing potential while keeping the problem analytically tractable: the deceleration  $-\frac{dv}{dt}$  is simply proportional to the satellite mass  $m(t)$  and the ambient density  $\rho(r, t)$  of the host galaxy at the time  $t$ . Without massloss Chandrasekhar’s formula would predict very efficient braking of the orbits, enough to make a high-mass satellite of  $\sim 10^{10} M_{\odot}$  (the mass of the LMC or M33 sized object) to decay from a circular orbit at  $\sim 100\text{kpc}$  to the very center of a high brightness galaxy in a Hubble time, delivering remnants into the inner galaxy. Here we study the effect of massloss and growing potential on the result of orbital decay, and the distribution of remnants. We present fully analytical results for calculating the decay rate for satellites on eccentric orbits in a scale-free growing isothermal potential.

The structure of the paper is following: S2 gives the analytical formulation of the problem, S3 presents results of application to globulars and dwarf satellites, S4 studies the relation between massloss and the satellite density profile. S5 discusses the progenitors of Sgr and  $\omega$ -Centauri, and S6 summarizes.

## 2. Analytical orbital decay model for a shrinking satellite in a growing host

Consider a satellite moving with a velocity  $\mathbf{v}_s$  on a rosette-like orbit in a spherical host galaxy potential  $\phi(r, t)$  with a rotation curve  $V_{\text{cir}}$ . Assume it has an initial mass  $m_i$ , the orbital decay from an initial time  $t = t_i$  to the present day  $t = t_0$  can be modeled using Chandrasekhar’s dynamical friction formula (Binney & Tremaine 1987)

$$\frac{d\mathbf{v}_s}{dt} = -\frac{\mathbf{v}_s}{t_{\text{fric}}} - \frac{V_{\text{cir}}^2}{r^2} \mathbf{r} \quad (1)$$

where  $t_{\text{fric}}$  is the instantaneous dynamical friction time. Manipulating the equation, we find the (specific) angular momentum  $\mathbf{j}(t)$  of the satellite decays as

$$\frac{d\mathbf{j}(t)}{dt} = \mathbf{r} \times \frac{d\mathbf{v}_s}{dt} = -\frac{\mathbf{j}(t)}{t_{\text{fric}}}, \quad \mathbf{j}(t) = \mathbf{r}(t) \times \mathbf{v}_s(t). \quad (2)$$

Here the dynamical friction time is given by

$$t_{\text{frc}}^{-1} = [4\pi G\rho(r, t)] \frac{Gm(t)}{V_{\text{cir}}^3} \xi(u), \quad u(t) \equiv \left( \frac{|\mathbf{v}_s|}{V_{\text{cir}}} \right) \quad (3)$$

where  $m(t)$  is the mass of the satellite,  $\rho(r, t)$  is the density of host galaxy at the orbital radius  $r(t)$ , and the effect of the satellite speed  $|\mathbf{v}_s|$  is contained in  $\xi(u)$ , which is some dimensionless function of the rescaled satellite speed  $u$ .

Here we adopt a Singular Isothermal Spherical (SIS) host galaxy model with a rotation curve generally growing with time  $V_{\text{cir}}(t)$ ; it is normalized by the present time value  $V_{\text{cir}}(t_0) = V_0$ . In this model the potential and density are given by

$$\phi(r, t) = V_{\text{cir}}^2(t) \ln r, \quad \rho(r, t) = \frac{V_{\text{cir}}^2(t)}{4\pi G r^2}. \quad (4)$$

Since the stars and dark matter velocity distribution in the host galaxy is an isotropic Gaussian, the dimensionless velocity function

$$\xi(u) = u^{-3} \left[ \text{erf}(u) - \frac{2u}{\sqrt{\pi}} \exp(-u^2) \right] \ln \Lambda \approx \frac{\ln \Lambda}{\frac{4}{3} + u^3}, \quad (5)$$

where the dimensionless Coulomb logarithm  $\ln \Lambda$  is typically between unity and ten. It is easy to verify that our *simple approximation* for  $\xi(u)$  works to 10% accuracy for  $0 \leq u = \left( \frac{|\mathbf{v}_s|}{V_{\text{cir}}} \right) < \infty$ , which is accurate enough in practice because real velocity distributions are often slightly non-Gaussian anyway. Note for very low speed  $\frac{\xi(0)}{\ln \Lambda} = \frac{4}{3\sqrt{\pi}} \approx \frac{3}{4}$  and for circular motion  $\frac{\xi(1)}{\ln \Lambda} = \text{erf}(1) - \frac{2}{e\sqrt{\pi}} \approx \frac{3}{7}$ .

Combining the above equations we find the decay rate for (the amplitude of) the angular momentum is given by <sup>3</sup>

$$\frac{dj(t)}{dt} = -\frac{j(t)}{t_{\text{frc}}}, \quad \frac{1}{t_{\text{frc}}} = \frac{G\mu(t)V_{\text{cir}}(t)}{j(t)^2}, \quad (6)$$

where we define an effective bound mass of the satellite at time  $t$

$$\mu(t) \equiv m(t)\beta(t), \quad \beta(t) = \xi(u)u^2 \cos^2(\alpha), \quad (7)$$

where  $u(t) = \frac{|\mathbf{v}_s(t)|}{V_{\text{cir}}(t)}$  and  $\alpha(t)$  are the rescaled speed and the pitch angle of the orbit at time  $t$ . As we can see, the effective mass  $\mu(t)$  lumps together several time-varying factors. It is

---

<sup>3</sup>the dynamical friction time  $t_{\text{frc}}$  is now expressed in terms of the angular momentum  $j(t)$  instead of  $r(t)$  with the help of substitutions  $r(t) \rightarrow j(t)/[|\mathbf{v}_s(t)| \cos \alpha(t)]$  and  $|\mathbf{v}_s(t)| \rightarrow u(t)V_{\text{cir}}$ .

proportional to the satellite mass  $m(t)$  by a dimensionless factor  $\beta(t)$  which incorporates the varying efficiencies of dynamical friction in an orbital epicycle. Note  $\beta(t)$  is an oscillating function of time of order unity, which we will come to in section 2.2. Introducing this *effective* mass simplifies the physics details because the braking rate of specific angular momentum  $-dj(t)/dt$  is now simply proportional to  $\mu(t)$ .

Integrating over time, we find the change in the specific angular momentum between time  $t_i$  to  $t_0$  is given by

$$-\Delta j^2 = j^2(t_i) - j^2(t_0) = 2G\mu_i V_0 \tau, \quad \tau \equiv (t_i - t_0)\gamma \equiv \int_{t_i}^{t_0} \frac{\mu(t)V_{\text{cir}}(t)}{\mu_i V_0} dt, \quad (8)$$

where we define  $\gamma$  as the reduction factor from fixed-mass satellite model, and define  $\tau$  as the effective duration of dynamical friction,  $\mu_i$  and  $V_0$  are the effective mass at initial time  $t_i$  and the rotation curve at the present  $t_0$ . The above formula allows us to calculate the evolution of the specific angular momentum  $j(t)$  of a generally *eccentric satellite orbit*.

It is interesting to ask what the necessary condition is for an outer halo satellite to reach the inner galaxy or even the center. These satellites will be destroyed with their remnants in the inner galaxy, e.g., by the disk and/or bulge shocking. To facilitate the comparison with observations, it is sometimes better to define an instantaneous orbital size <sup>4</sup>

$$S(t) \equiv \frac{j(t)}{V_0} \quad (9)$$

at time  $t$ . Let the present orbital size  $S_0 = \frac{j_0}{V_0} \leq R_{\text{disk}} \sim 15\text{kpc}$ , and define  $j_{\text{disk}} = R_{\text{disk}} \times V_0$  as the critical angular momentum to reach within the disk at the present time. Manipulating eq. (8) we find the initial angular momentum  $j_i$  or orbital distance  $S_i = \frac{j_i}{V_0}$  must satisfy

$$S_i = \left[ S_0^2 + \frac{2G\mu_i\tau}{V_0} \right]^{\frac{1}{2}}, \quad 0 \leq S_0 \leq R_{\text{disk}}, \quad (10)$$

where  $\tau$  is given in eq. (8). In other words, satellites initially on orbits larger than  $S_i$  would not be able to deliver a globular or dwarf galaxy to the inner galaxy irrespective of mass loss assumed.

---

<sup>4</sup>We can make this definition irrespective of the eccentricity of the orbit, which we does not enter our calculation explicitly. Roughly speaking the orbital size  $S(t)$  is the geometrical mean of the pericenter radius and apocenter radius in a static potential.

## 2.1. A geometrical interpretation

Eq. (8) is our main analytical result. There is also an interesting geometrical interpretation to it. Consider, for example, a satellite of mass  $m(t)$  on a *circular orbit* in a static SIS potential, we have

$$\ln \Lambda \approx 2.5, \quad \beta(t) = \xi(1) \times 1^2 = 0.42 \ln \Lambda \approx 1, \quad \mu(t) = m(t)\beta(t) \approx m(t), \quad (11)$$

where we took a typical value for the Coulomb logarithm (e.g., Penarrubia, Kroupa & Boily 2002). We can rewrite the angular momentum equation (eq. 8) as

$$|\pi \Delta S^2| \approx \frac{2\pi G \langle m \rangle}{V_0^2} (V_0 \Delta t), \quad \langle m \rangle = \frac{\int_{t_i}^{t_0} m(t) dt}{t_0 - t_i} \quad (12)$$

where the l.h.s. is the area swept by the decaying orbit, and in the r.h.s.  $2\pi G \langle m \rangle V_0^{-2}$  is the "circumference of influence" of the satellite, and the  $V_0 \Delta t = V_0(t_0 - t_i)$  is the length of the satellite's orbital path, and the multiplication of the two is the area swept by the circumference of influence of the satellite. The above equation implies that the two areas are comparable. Interestingly the decay of the orbits depends on the satellite mass through the approximation  $\Delta S^2 \propto \langle m \rangle \Delta t$ , i.e., it is the average mass of the satellite that determines the rate of orbital decay. Finally note eq.(8) applies to the evolution of specific angular momentum of an eccentric orbit in a time-varying potential. A complete description of the orbits should also include the evolution of the orbital energy, which unfortunately is more complex analytically, and is not studied in detail here. It is not essential for our conclusion, but is perhaps convenient to assume efficient dynamical decay of the orbital energy during the pericentric passages hence the radial motion is damped and orbit circularizes at the end. Adiabatic growth of the potential also tends to circularize the orbits.

## 2.2. Modeling the growing host potential

Classical singular isothermal model assumes a fixed potential or a time-invariant rotation curve. In reality galaxies grow substantially from redshift of a few to now. The growth of the dark halo is scale-free in the hierarchical scenario, so it is plausible to approximate the growth of the rotation curve as a power-law in time as follows,

$$V_{\text{cir}}(t) = V_0 \left( \frac{t}{t_0} \right)^p, \quad 0 < t < t_0, \quad (13)$$

where the rotation speed at some earlier time  $0 < t < t_0$  is generally smaller than the present day ( $t = t_0 = 14\text{Gyr}$ ) value  $V_0$ . At the present epoch  $V_{\text{cir}}(t_0) = V_0 = 200 \text{ km s}^{-1}$  is

appropriate for the Milky Way. A few sample evolution models are shown in Fig.1a. A value of  $\frac{1}{9} \leq p \leq \frac{1}{3}$  implies an evolution of 10%-25% in rotation speed from redshift one to now, which seems reasonable in models of the Milky Way before and after the formation of the disk and the bulge (Klypin, Zhao, Somerville 2001; Wright 2003).

### 2.3. Modeling the shrinking satellite

Previously the tidal stripping of the satellite is either modeled by N-body simulations (e.g., Tsuchiya et al. 2003, 2004, Johnston et al. 1999) or semi-analytically using tidal radius criteria (e.g., Zhao 2002, Kendall, Magorrian & Pringle 2003).<sup>5</sup> In both approaches one needs to assume a rigorous description of the mass profile of the progenitor satellite. It is unclear whether this approach can model efficiently the realistic large scatter in the circular velocity curves of observed dwarf galaxies.

Here we take a very different approach. We model the mass of the progenitor galaxy as a simple function of time with two free parameters. We do not need an explicit prescription of the satellite density profile. Motivated by the massloss history typically seen in N-body simulations, the satellite mass is modeled to decay in a rate between exponential and linear massloss. To simplify the calculations, we lump together several uncertain factors, and simply assume the *effective* mass of the satellite is shed following the following recipe,

$$\begin{aligned} \mu(t) &= \langle\beta\rangle_i m_i \left\{ 1 - \left[ 1 - \left( \frac{\langle\beta\rangle_0 m_0}{\langle\beta\rangle_i m_i} \right)^{\frac{1}{n}} \right] \hat{t} \right\}^n, \quad \hat{t} = \frac{t - t_i}{t_0 - t_i}, \\ m(t) &= m_i \left\{ 1 - \left[ 1 - \left( \frac{m_0}{m_i} \right)^{\frac{1}{n}} \right] \hat{t}_N \right\}^n, \quad \hat{t}_N = \hat{t} - \frac{\sin 2N\pi\hat{t}}{2N\pi} \approx \hat{t}, \end{aligned} \quad (14)$$

where  $m_0$  and  $m_i$  are the mass at the present  $t = t_0 = 14\text{Gyrs}$  and when the satellite falls in  $t = t_i$ , and  $0 \leq \hat{t} \leq 1$  is the rescaled dimensionless time, and  $N \sim 1 - 100$  is the total number of pericentric passages between time  $t_0$  and  $t_i$ . The parameters  $\langle\beta\rangle_i$  and  $\langle\beta\rangle_0$  are the initial and final effective mass conversion factors, which we will come to.

The parameter  $n$  determines the profile of the massloss history. It is tunable with the  $n = 1$  model having a constant rate of massloss, and the  $n \rightarrow \infty$  having an exponential massloss; and  $n = -1$  is a roughly power-law decay. In simulations we typically see somewhere in

---

<sup>5</sup>Recently the latter approach has also been extended to model the orbital decay and evaporation-induced massloss in the dense star cluster near the Galactic center (Mouri & Taniguchi 2003, McMillan & Portegies-Zwart 2003).



between these cases:  $0 < n \leq 1$  for Plummer or King model satellites with a sharp fall off after an initially linear massloss (e.g., Penarrubia et al. 2002); for isothermal satellite models, the massloss is close to linear  $n = 1$  (Zhao 2002). Note for a completely disrupted satellite  $m_i \gg m_0 \sim 0$ . In N-body simulations satellite losses mass mainly in bursts near pericentric passages, so the mass is a descending staircase like function of time. This is simulated fairly well by our formula with  $\hat{t}_N$  in  $m(t)$ : a few example massloss histories are shown in Fig.1a where we assume  $N = 10$  pericentric passages from  $t_i = 4\text{Gyr}$  to now  $t_0 = 14\text{Gyr}$ .

#### 2.4. Modeling the effective mass conversion factor $\langle \beta \rangle$

The conversion factor between the effective mass  $\mu(t)$  and the actual mass  $m(t)$  of the satellite is given by

$$\beta(t) = \frac{\mu(t)}{m(t)} = \xi(u) (u \cos \alpha)^2, \quad (15)$$

where  $u$  is the rescaled satellite velocity at time  $t$  and  $\alpha(t)$  is the pitch angle. To compute the average value of  $\beta(t)$  over one epicycle, let us first define  $C$  as the ratio of the apocenter  $r_a$  to pericenter  $r_p$ , or the ratio of pericenter velocity  $u_a V_{\text{cir}}$  and  $u_p V_{\text{cir}}$ , where

$$u_p V_{\text{cir}} = \frac{j}{r_p}, \quad C \equiv \frac{r_a}{r_p} = \frac{u_p}{u_a}. \quad (16)$$

According energy conservation we have

$$\frac{E}{V_{\text{cir}}^2} = \frac{u_p^2}{2} + \ln r_p = \frac{u_a^2}{2} + \ln r_a, \quad (17)$$

where  $E$  is the energy at pericenter and apocenter. It is easy to show that  $r_p$  and  $u_p$  are determined by the angular momentum  $j$  and the circular velocity  $V_{\text{cir}}$  as follows,

$$r_p = j V_{\text{cir}}^{-1} u_p^{-1}, \quad u_p = \sqrt{\frac{2 \ln C}{1 - C^{-2}}}. \quad (18)$$

Now if we make the approximations that

$$\frac{\mu(t)}{m(t)} \approx \langle \beta(t) \rangle \approx \xi(\langle u \rangle) \langle u^2 \cos^2 \alpha \rangle \quad (19)$$

and the further approximations

$$\langle u^2 \cos^2 \alpha \rangle \approx u_p u_a \quad \langle u \rangle \approx \left( \frac{u_p^{2k} + u_a^{2k}}{2} \right)^{\frac{1}{k}}, \quad k = \frac{9}{11} \quad (20)$$

then we have

$$\frac{\mu(t)}{m(t)} \approx \langle \beta(t) \rangle \approx \xi \langle \langle u \rangle \rangle \cdot \left( \frac{2 \ln C}{C - C^{-1}} \right), \quad \langle u \rangle = \frac{C^k + C^{-k}}{2} \left( \frac{2 \ln C}{C - C^{-1}} \right)^k, \quad k = \frac{9}{11} \quad (21)$$

Eq. (21) is then checked with the time averages computed by direct numerical integration of the orbit from pericenter to apocenter, and is found to be accurate to 2% for  $1 \leq C \leq 100$  (A simpler expression with  $k = 1$  gives somewhat poorer accuracy). While we neglect variation of  $\beta$  within one epicycle, there can still be secular evolution because the orbital energy is lost more efficiently at pericenter, hence the orbit tends to circularize, which increases the effective mass conversion factor  $\langle \beta \rangle$ . Generally speaking the factors  $\langle \beta \rangle$ ,  $u_p$  and  $u_a$  etc. are functions of  $C$ , which can be read out from the curves in Fig.1b. For those Milky Way satellites and globular clusters which we have good proper motions, the C-values are typically between 1 and 10 (Dinescu et al. 1999), hence  $\langle \beta \rangle$  varies only by a factor of at most three for these satellites. So the uncertainty of their effective masses  $\mu = \langle \beta \rangle m$  is still largely from errors of their observed mass-to-light ratios.

The above conversion factor should be a good approximation for eccentric satellite orbits with apo-to-peri ratio of  $C$  in a flat rotation curve potential. For example, for an apo-to-peri ratio  $C = \frac{r_a}{r_p} = 5$ , we have a rescaled pericenter speed  $u_p \approx \sqrt{3}$ , and an average mass conversion factor  $\langle \beta \rangle \approx 0.5 \times (0.42 \ln \Lambda)$ . Assume  $\ln \Lambda = 2.5$  we have  $\mu(t) \approx 0.5m(t)$ . In comparison  $\mu(t) \approx m(t)$  for circular orbits. So for the same angular momentum, our model suggests that eccentric orbits have smaller effective mass of the satellite, hence slower evolution of the orbital angular momentum.<sup>6</sup> It is interesting that all three factors: mass loss, growing potential, and orbital eccentricity all work in the same sense of reducing the evolution of orbital angular momentum.

For a rough estimation of the reduction of dynamical friction due to satellite mass loss and host growth, let's consider a *Gedanken* experiment where a satellite enters a growing host galaxy at time  $t_i = 0$  right after the big bang and is completely dissolved ( $\mu_0 = 0$ ) by the time  $t_0$ . Neglecting the sinusoidal component by letting  $N \rightarrow \infty$ , the reduction factor  $\gamma$  is computed by substituting eqs. (13-14) into eq. (8). We find  $\gamma = \frac{p!n!}{(p+n+1)!} = \frac{1}{6}$  if the satellite loses mass linearly with time ( $n = 1$ ) in a linearly growing halo ( $p = 1$ ). This estimate is perhaps to the extreme. In reality the formation and mergers of the satellites are probably over an extended period of the Hubble time, perhaps starting around redshift of 1.5 ( $t_i = 4\text{Gyr}$ ), ending around now ( $t_0 = 14\text{Gyr}$ ). Hereafter we consider mostly models with  $t_i = 4\text{Gyr}$ , and  $t_0 = 14\text{Gyr}$ ,  $0 \leq p \leq \frac{1}{3}$  and  $\mu_0 \ll \mu_i$ .

---

<sup>6</sup>However, the circularization of orbit tends to enhance dynamical friction.

### 3. Results of application to globulars and dwarf satellites

Section 2 gives the formalism to predict analytically the evolution of the angular momentum of the satellite for a satellite with any massloss history on an eccentric orbit around a time-varying potential.

Clearly not all satellites could reach the galactic center as a globular or a naked massive black hole. Dynamical friction is basically turned off if the satellite bound mass drops below  $10^9 M_\odot$  before reaching the inner galaxy. To reach the inner, say, 15 kpc of the host galaxy, which is roughly the truncation radius of the outer disk of the Milky Way, a satellite must have presently a specific angular momentum

$$0 \leq j_0 \leq j_{\text{disk}} \equiv R_{\text{disk}} V_0 = 15 \text{kpc} \times 200 \text{ km s}^{-1}. \quad (22)$$

In comparison the present specific angular momentum of some of the known satellites are given in Table 1. The Magellanic stream and Ursa Minor have  $j_0 \sim 15000 \text{ km s}^{-1} \text{kpc}$  much larger than  $j_{\text{disk}}$ .

Suppose there was a population of hypothetical dwarf satellites in the outer halo with a specific angular momentum comparable to that of the orbits of LMC, Ursa Minor and Fornax. Suppose their initial mass  $m_i$  is between Ursa Minor and the LMC ( $10^7$ – $10^{10} M_\odot$ ) at sometime  $t_i$  between 4 – 14 Gyr. We integrate forward in time to answer the question where their remnants are. Clearly the effect of orbital decay is maximized if we take the longest evolution time (10 Gyr), the highest initial satellite mass and smallest initial orbit  $j_i = 60 \text{kpc} \times 250 \text{ km s}^{-1}$ . This is the case shown by the hatched region in Fig. 2 with the satellite starting from the upper right corner and ending to the lower left with a mass  $10^7 M_\odot$ . The vertical axis  $S(t) = j(t)/200$  is a characteristic orbital distance of the satellite, expressed in terms of the specific angular momentum divided by a characteristic velocity  $200 \text{ km s}^{-1}$ . This orbital distance is roughly the geometrical mean of the apocenter and pericenter. Models are shown in order of increasing dynamical braking. The upper shaded zone are models with between exponential and linear massloss and a moderate evolution of the potential ( $\infty \geq n \geq 1, p = \frac{1}{3}$ ), the lower shaded zone are models with between linear to accelerated massloss and a static potential ( $1 > n > 0.3, p = 0$ ). Qualitatively speaking the orbital decay appears to be only modest in all cases, the remnants are generally not delivered to the inner galaxy.

The condition for a satellite to deliver a low-mass substructure to the inner halo (cf. eq.15) or a  $10^6 M_\odot$  black hole to the galaxy center is summarized in Fig.3. The satellite must be within 20 kpc for the past Hubble time for a low-mass ( $10^7$ – $10^9 M_\odot$ ) progenitor. It could be at a modest distance of 40-50 kpc if the progenitor was very massive ( $10^{10} M_\odot$ ) with a linear or accelerated massloss ( $n < 1$ ) and little evolution of the galactic potential ( $p \ll 1$ ).

Progenitors of the inner halo substructures or central black hole cannot be on orbits of specific angular momentum comparable to the LMC, Ursa Minor or Fornax. This illustrates the difficulty of making systems such as  $\omega$ -Centauri as the nucleus of a stripped-off dwarf galaxy starting from the very outer halo. Likewise it is difficult for a minor merger to bring in a million solar mass black hole to the host galaxy center. The progenitor’s orbit must be radial and well-aimed at the galaxy center such that the progenitor’s tangential velocity is  $\leq 1 \text{ km s}^{-1}$  if the satellite comes from an initial distance of 1Mpc.

#### 4. Comparison of various models for tides and satellite density profiles

The basic feature of our dynamical friction models is that they bypass any information of the satellite internal density profile and the varying tidal force on the satellite by specifying the effective mass  $\mu(t)$  as an explicit empirical function of time directly. This immediately brings up two questions, which we answer in the next two subsections: (1) Is our analytical model accurate enough? Compared to a simulation with the more traditional ”tidal peeling” approach, does our model reproduce the overall rate of the orbital decay for the same initial conditions? (2) Can our analytical model be used to infer the underlying mass profile for satellites? Is the inferred mass profile plausible for observed satellites?

##### 4.1. Inferring satellite rotation curves and comparing with observations

Indeed we can infer the internal mass distribution, or internal circular velocity curve, of the satellite using the tidal radius criteria. More specifically the internal circular motion  $v_{\text{cir}}$  at the tidal radius  $r_t(t)$  should be in resonance with the satellite’s orbital frequency at the pericenter  $r_p(t)$ , meaning that their angular frequencies or time scales are equal with

$$\frac{r_t}{v_{\text{cir}}} = t_{cr} = \frac{r_p}{V_{\text{cir}}}, \quad (23)$$

where  $t_{cr}$  is the crossing time, and the radii

$$r_t(t) = \frac{Gm(t)}{v_{\text{cir}}^2}, \quad r_p(t) = \frac{j(t)}{u_p V_{\text{cir}}}, \quad (24)$$

where the factor  $u_p$  is the boosting factor of the pericenter velocity due to eccentricity. If we define  $\rho_t$  as the satellite’s overall mean density at tidal radius  $r_t$ , and  $\rho_{amb}$  and  $M(t)$  as the average ambient density and the total mass inside the pericenter  $r_p$ , then

$$m(t) = \frac{4\pi\rho_t r_t^3}{3}, M(t) = \frac{4\pi\rho_{amb} r_p^3}{3} = \frac{V_{\text{cir}}^2 r_p}{G}, \quad (25)$$

Eliminate  $r_p$  and  $r_t$  with substitutions, we can rewrite the tidal criteria (eq. 23) as follows

$$\left(\frac{4\pi G\rho_t(t)}{3}\right)^{-\frac{1}{2}} = t_{cr} = \left(\frac{4\pi G\rho_{amb}(t)}{3}\right)^{-\frac{1}{2}} \quad (26)$$

This means that as time progresses, the satellite mass  $m(t)$  decreases (eq. 8), its orbital pericenter  $r_p(t)$  decreases (eqs. 14, 24), the satellite’s mean density  $\rho_t(t)$  increases with the ambient density  $\rho_{amb}$  (eq. 26), hence the tidal radius  $r_t(t)$  shrinks with the satellite’s mass  $m(t)$ , like what happens with peeling off an onion. The tidal peeling-off process effectively maps out  $\rho_t$  as a function of  $m$  implicitly through these equations. The function  $\rho_t(m)$  can then be converted to the internal mass radial profile of the satellite since  $r_t(m) \propto [m/\rho_t(m)]^{1/3}$ . The circular velocity as a function of enclosed mass  $m$  can then be calculated with  $v_{\text{cir}}^2(m) = Gm/r_t(m)$ .

The relation between  $v_{\text{cir}}$  and the mass  $m(t)$  can also be shown more explicitly as follows. From the tidal criteria (eq. 23) we have

$$j(t) \propto r_p(t)V_{\text{cir}} \propto V_{\text{cir}}^2 v_{\text{cir}}^{-1} r_t \propto V_{\text{cir}}^2 v_{\text{cir}}^{-3} m(t) \quad (27)$$

since the tidal radius  $r_t = Gmv_{\text{cir}}^{-2}$  (cf eq. 24). Substitute in the orbital evolution equation (eq. 6), and assume  $\mu(t) \propto m(t)$ , we have

$$\frac{d}{dt} [mV_{\text{cir}}^2 v_{\text{cir}}^{-3}] \propto \frac{dj(t)}{dt} \propto \frac{m(t)V_{\text{cir}}}{j(t)} \propto V_{\text{cir}}^{-1} v_{\text{cir}}^3. \quad (28)$$

So there is a one-to-one relation between the massloss history  $m(t)$  and the circular velocity at the tidal radius  $v_{\text{cir}}$  if we fix the host potential ( $V_{\text{cir}} = cst$ ). Interestingly this explains why a satellite with flat rotation  $v_{\text{cir}} = cst$  leads to a linear mass loss history  $\frac{d}{dt}m(t) = cst$ .

A few circular velocity curves are shown in Fig.4 and Fig.5. First we consider a hypothetical globular cluster of  $10^6 M_\odot$  on an orbit of apo-to-peri ratio of 15 kpc : 3 kpc, which is within the inner galaxy although a slightly bigger orbit than  $\omega$ -Centauri . If this cluster is the end result of, say, losing mass linearly with time from a  $10^{10} M_\odot$  progenitor a Hubble time ago, then the tidal criteria implies a mass profile of the progenitor, shown by the circular velocity curve (labelled  $n = 1$ ) in Fig.4b. The progenitor must have a velocity curve close to that of an isothermal cored halo with a tidal radius  $r_t \sim 6.5$  kpc. This implies an initial pericenter of about  $r_p(t_i) = \frac{200 \text{ km s}^{-1}}{80 \text{ km s}^{-1}} r_t \sim 16$  kpc (cf. eq. 23). So the progenitor must start out on a small orbit with the first pericenter almost touching the inner halo of the host. Such an orbit is a much smaller than the one that the LMC and SMC are/were on, which has a pericenter about 40 kpc now and perhaps even further a Hubble time ago. This result holds qualitatively for a wide range of assumed massloss history. When we decrease  $n$

from 30 to 0.3, the inferred initial tidal radius increases from  $r_t = 4$  kpc to  $r_t = 7.5$  kpc (cf. Fig.4b), corresponding to a pericenter  $r_p = 8$  kpc to  $r_p = 20$  kpc. The LMC has tidal radius of about 8 – 10 kpc. So in order to deliver a final remnant to the inner 15 kpc, we must start with a much smaller orbit and a much denser satellite than the LMC.

It is also remarkable that our predicted circular velocity curves resemble very well those of observed dwarf galaxies, for a variety of initial and final parameters of the satellite and the host galaxy. Rotation curves are shown in Fig. 4a for several nearby dwarf galaxies of virial mass  $\sim 10^{10} M_\odot$ : DDO154 (Carnigan & Purton 1998), NGC3109 (Jobin & Carignan 1990), NGC5585 (Blais-Ouellette et al. 1999), NGC2976 (Simon et al. 2003). Also indicated (by the locations of the small open circles) are the core radius vs. the maximum rotation velocity for a sample of about 50 dwarf galaxies compiled in Sellwood (2000); only those with total mass less than  $10^{10} M_\odot$  are shown here.

The fact that our models give reasonable mass profiles of satellites justifies our empirical parametrization of the massloss history (eq. 14), and gives a *physical meaning to our n parameter*:  $n = 1$  resembles a cored isothermal model,  $n \gg 1$  gives an overall solid-body circular velocity curve, and  $n \ll 1$  gives a Keplerian-like curve with a dense solid-body core.

Observed dwarf galaxies typically have a solid-body core instead of a cold dark matter cusp, with the density bounded typically between  $0.25 - 0.0025 M_\odot \text{pc}^{-3}$ ; note the densest known dwarf galaxy Draco has a core density of  $0.7 M_\odot \text{pc}^{-3}$  (Sellwood 2000). These cores imply destruction of the typical dwarf galaxies once they decay to pericenters  $r_p = 3$  kpc – 30 kpc from a Milky Way host. Among the observed dwarf galaxies, those with a core density comparable or lower than  $0.01 M_\odot \text{pc}^{-3}$  (e.g., DDO154, NGC3109) would be torn into tidal streams before reaching 15 kpc of the galaxy.

Similar calculations are also done for a Sgr-like remnant of  $10^8 M_\odot$  on an orbit of 40 kpc : 8 kpc (Fig.5b). The results for the progenitor are shown and compared with the observed dwarfs in a log-log plot (Fig.5a). Again the progenitors resemble the observed dwarfs, but again the progenitor must originate from a small orbit.

#### 4.2. Comparing the analytical model with "tidal peeling" simulations

A key assumption of our model is that the effective mass is some simple empirical function of time (cf. eq. 14) with the normalization  $\langle \beta \rangle$  determined by the apo-to-perigalactic ratio (cf. eq. 21). In reality the satellite's mass is determined by the tides at the pericenter, and the dynamical friction force modulates periodically between pericenter and apocenter. However, these short-time-scale variations are smoothed out when averaged over a Hubble

time and almost do not contribute to the evolution of the orbital angular momentum.

To verify consistency of our empirical massloss history (eq. 14) with the tidal massloss history we recompute the orbital decay using traditional tidal conditions, similar to Jiang & Binney (2000) and Zhao (2002). Here we fix  $\ln \Lambda = 2.5$  and show only two general cases with a satellite with a LMC-like flat rotation curve of amplitude  $v_{\text{cir}} = 70 \text{ km s}^{-1}$  in a host halo of flat circular velocity curve of amplitude  $V_{\text{cir}} = 200 \left(\frac{t}{14}\right)^{\frac{1}{9}} \text{ km s}^{-1}$  (i.e.  $p = 1/9$ ). The satellite is launched on an eccentric orbit with initial specific angular momentum and apo-to-peri ratio being  $j_i = 45 \text{ kpc} \times 280 \text{ km s}^{-1}$  and  $C = 3$  for model A, and  $j_i = 20 \text{ kpc} \times 350 \text{ km s}^{-1}$  and  $C = 8$  for model B, starting from the pericenter (at  $r_p = 45 \text{ kpc}$  or  $20 \text{ kpc}$ ); the pericenter radius and speed are determined by  $C$  according to eq. (20), which then determines the initial tidal radius of the satellite (cf eq. 23), and the mass (cf eq. 24). The tidal criteria at the pericenters determines the evolution of the total mass of the satellite (cf. eq. 28), which should be slightly non-linear partly due to  $V_{\text{cir}} \propto t^{1/9}$  and partly due to circularization of the orbit. The satellite orbit is followed for 10 Gyrs and shown in Fig.6. The orbit shrinks and becomes more circular than initially due to dynamical friction and the satellite losses most of its initial mass. In Model A it shrinks from 120kpc/45kpc to 15/10kpc, and the mass is reduced by a factor of about 5. In Model B it shrinks from the initial apocenter/pericenter of 140kpc/20kpc to the final about 55kpc/15kpc and the mass is reduced by a factor of about 2.

This is compared with our analytical model for the mass and angular momentum. The initial and final mass of the satellites  $m_i$  and  $m_0$  are taken from the above tidal-peeling simulations, and also for the the initial and final apo-to-peri ratios  $C$ , which we convert to the initial and final values for  $\langle \beta \rangle (C)$  with the help of eq. (21) or Fig.1b; generally  $\langle \beta \rangle_i \leq \langle \beta \rangle_0$  because of circularization; together these specify the initial and final effective mass  $\mu(t_i)$  and  $\mu(t_0)$ . We then adopt a simple linear massloss  $n = 1$  law connecting the the initial and the final (effective) mass of the satellite. The tidal criteria (eq. 28) suggests that such a linear massloss model would be rigorous for circular orbit in a static potential ( $p = 0$ ) since the satellite and the galaxy both have flat rotation curves. We then substitute this massloss history in eq. (8) to predict the past angular momentum  $j(t)$  from the present (smaller) value  $j(t_0) = j_0$  backward. <sup>7</sup> The agreement of predictions from the two methods is clearly good overall (cf. Fig.6b). The agreement is poorer for higher eccentricity orbit with a stronger evolution in eccentricity. This is because our analytical method does not attempt to model the orbital circularization in any details apart from varying  $\langle \beta \rangle$ .

---

<sup>7</sup>Predicting  $j(t)$  from the initial (bigger) value  $j(t_i)$  forward would be less stable or accurate once  $j(t) \rightarrow 0$  because the relative error diverges.

We also check our models against previous fully self-consistent live-halo simulations, i.e., simulations using live particles to represent the halo of our galaxy. we convert the initial conditions of these simulations to calculate  $S_i$  and  $\mu_i$ . This is shown in Fig.3. The three simulations (Model A, F, K) of Jiang & Binney (2000) require a very massive ( $10^{10-11}M_\odot$ ) progenitor of the Sgr far away (150 – 250 kpc) from our Galaxy with an initial angular momentum consistent with our linear massless model ( $n = 1$ , heavy dashed). Here we adopt initial apo-to-peri ratio  $C \sim \frac{200 \text{ kpc}}{60 \text{ kpc}}$  and  $\langle\beta\rangle_i = 0.6$  from their simulations. Jiang & Binney have also done semi-analytical modeling of orbital decay, and they find models with  $\ln \Lambda = 8.5$  fit best. The discrepancy with our preferred value for  $\ln \Lambda \sim 2.5$  are likely due to differences in details of the analytical modeling: their Milky Way halo model has an exponential truncation beyond 200 kpc, which reduces the halo’s density and dynamical friction at 150 kpc – 250 kpc by about one e-folding. Their definition of the tidal radius also implies a systematically stronger (up to a factor of two for Model A initially) tide hence somewhat smaller satellite. Also their semi-analytical satellites loss mass somewhat faster than linear.

A rough agreement is also seen with self-consistent simulations of  $\omega$ -Centauri , where we adopt  $C = \frac{60 \text{ kpc}}{1 \text{ kpc}}$  hence  $\langle\beta\rangle_i = 0.015$  for the best fit H4 model by Tsuchiya et al. (2003), and  $C = \frac{26 \text{ kpc}}{6 \text{ kpc}}$  hence  $\langle\beta\rangle_i = 0.45$  for Bekki & Freeman (2003). There is some discrepancy with Bekki & Freeman, perhaps due in part to our neglecting effects of the disk. The final phase of their merger model is perhaps too violent for ChandraSekhar’s analytical description anyway. Indeed their orbit did not circularize, instead the apo-to-peri ratio increased to 8 kpc : 1 kpc, somewhat larger than the observed orbit of  $\omega$ -Centauri . Correcting down their orbital size would make better agreement with our prediction.

## 5. Discussions

### 5.1. Effects of disk, bulge and orbital inclination

One limitation of the current analysis is that we assume an isothermal dark matter plus stars model throughout the galaxy, hence the dynamical friction effect of the disk and bulge are not modeled accurately. However, the disk and bulge are not important for our conclusion because we predict mainly the orbital decay in the outer halo where  $j > j_{\text{disk}} = 3000 \text{ kpc km/s}$ . Inside 15 kpc, our estimation of dynamical friction by an SIS model is inaccurate only for satellites on low inclination orbits. If satellites come in random inclinations, it is more common to find high inclination orbits, for which our models should be fairly accurate even inside 15 kpc.



## 5.2. Effects of escaping stars

In the part of our formulation where we derive the satellite mass profile, we assume a simplifying static picture that the satellite’s mass is peeled off in successive layers at the shrinking tidal radius. The picture in N-body simulations is more complicated, since satellite particles at all radii, e.g., the center of the satellite, could in principle be escaping at any time. So eq. (26) sets only a lower limit on the initial density of the satellite. A more rigorous model should making this correction, e.g., by introducing an empirical factor to correct this as in Jiang & Binney (2000).

## 5.3. Possible orbits of progenitors of the Sgr stream

The Sgr dwarf and the Canis Major dwarf are the closest known dwarf galaxies, about 15 kpc from the center of the Milky Way and at the edge of the Milky Way disk. The Canis Major is on a (direct or retrograde) orbit slightly inclined from the plane of the Milky Way, and the Sgr is on a nearly polar orbit. Both orbits have a fairly low angular momentum with  $S \sim 20$  kpc; the data on Sgr are more complete, and show that it oscillates between 10 kpc pericenter and 50 kpc apocenter. Both contain several globular clusters. It is possible that the two dwarfs are the stripped-down version of a more massive object, which has dynamically decayed from the outer halo.

Interestingly a possible extension of the Sgr has been reported recently in the SDSS data near the position of the outer halo globular cluster NGC2419 (Newberg et al. 2003). There is a stream-like enhancement of halo A-colored stars at the SDSS magnitude of  $g_0 = 20.3$  in the plane of the Sgr’s orbit, corresponding to a distance of 90 kpc. If this is true, it would imply that the Sgr has changed its orbits in the past Hubble time. There are two possible ways that this could happen. One is that the Sgr’s orbit has been deflected by a massive satellite, such as the LMC or SMC. Indeed the orbits of the Sgr and the Magellanic Clouds do overlap at the Galactic poles, and simple timing arguments show that these systems encounter or fly by each other about 2.5 Gyrs ago at about 50 kpc on the North Galactic Pole if the rotation curve of the Milky Way is nearly flat (Zhao 1998). The problem of this solution is that it is rare for the Sgr to receive a strong enough deflection to bring down its orbit.

Another solution is that the Sgr has been a more massive system, which orbital decayed from the outer halo (Jiang & Binney 2000). *Our Model B illustrates such an example of the progenitor of the Sgr* which had an initial mass comparable to the LMC ( $10^{10} M_{\odot}$ ) and was on an eccentric orbit with radius between 20 – 140 kpc (cf Fig.6). This model is similar to the Model K of Jiang & Binney. After a Hubble time the orbit decays to a small orbit very much

like that of the Sgr with peri-to-apo ratio of 10 kpc : 50 kpc. Large amount of the material of the progenitor is shed in the radius between 10 – 140 kpc, the stream near NGC2419 at 90 kpc could be part of this debris near one of the apocenters of the orbit. Unfortunately the present model ends with a mass of  $5 \times 10^9 M_\odot$ , too large for the present-day Sgr. Some fine tuning of initial conditions and detailed N-body simulations are clearly needed to test this idea.

#### 5.4. Possible orbits of the progenitor of $\omega$ -Centauri

We have mainly concentrated on the problem of getting rid of a satellite’s angular momentum if it starts with a high angular momentum or orbital size  $S_0 \gg 15\text{kpc}$ . What would be the remnant distribution if a satellite is born with an initial orbital size  $S_i < 15\text{kpc}$ ? The stars in such a system are assembled in the inner halo from the start, e.g., by colliding an infalling gas cloud with the protogalactic gas clouds in the inner halo, (Fellhauer & Kroupa 2002). Or the stars form from extragalactic gas and descend on a very radial orbit, penetrating the inner 15 kpc of the host halo from its very first pericentric passage.

An intriguing example is  $\omega$ -Centauri . Unfortunately our analytical model is not suited for this system because it is presently on a low-inclination eccentric retrograde orbits between 1 and 6 kpc from the Galactic center (Dinescu et al. 1999), so the contribution of dynamical friction by the disk is important. Also hydrodynamical friction with the disk gas can play a role for an early-on partially gaseous satellite. Nevertheless, if one applies simplistically the tidal massloss and Chandrasekhar’s dynamical friction in a spherical halo, one finds that while it seems easy to peel off a satellite galaxy to make a central star cluster, most simulations produce remnants on much larger orbits than  $\omega$ -Centauri (Zhao 2002). It seems some fine tuning is required to select progenitors on very low angular momentum and/or low energy orbits: the initial angular momentum needs to be low enough for the progenitor to penetrate into the inner halo or the present location of  $\omega$ -Centauri on its very first pericentric passage. This means that the initial orbital size  $S_i^\omega$  of  $\omega$ -Centauri is in between the present value of  $\omega$ -Centauri  $S_0 \sim 1.25\text{kpc}$  and the boundary of the inner halo  $R_{\text{disk}} = 15\text{kpc}$ , or mathematically

$$1.25 \text{ kpc} < S_i^\omega < 15 \text{ kpc}. \quad (29)$$

Most recently there have been several very encouraging attempts to model the dynamical and star formation history of  $\omega$ -Centauri by nearly self-consistent N-body simulations (Mizutani et al. 2003, Tsuchiya et al. 2003, Bekki & Freeman 2003). All are able to produce both a reasonable mass and orbit of the  $\omega$ -Centauri after some trial and error with the initial parameters of the progenitor; many initial conditions lead to remnants, unlike  $\omega$ -Centauri ,

beyond 10kpc of the Milky Way center. The favored initial orbit has a small orbital size  $S_i$ , according to Tsuchiya et al.  $j_i = 60\text{kpc} \times 20 \text{ km s}^{-1} = 1200\text{kpc km s}^{-1}$  (or  $S_i = 6\text{kpc}$ ) and according to Bekki & Freeman  $j_i = 25\text{kpc} \times 60 \text{ km s}^{-1} = 1500\text{kpc km s}^{-1}$  (or  $S_i = 7.5\text{kpc}$ ). The small orbital size seems consistent with our expectation (cf. Fig.3).

Tsuchiya et al. launch satellites with various initial mass  $(0.4 - 1.6) \times 10^{10} M_\odot$  and with either a King profile or a Hernquist profile from 60 kpc from the Milky Way center. They choose well-aimed nearly radial orbits, with an initial perigalactic radius about 1 kpc, much more radial than the present eccentric orbit. Massloss in their King model are similar to our exponential massloss models ( $n = \infty$ ): rapid in the beginning, and  $\log(m)$  is roughly linear with time up to a mass of  $10^8 M_\odot$  when the satellite has too little mass to proceed with the orbital decay. Massloss in the Hernquist model is closer to a  $n = 0.3$  model, linear in the beginning and rapid just before complete disruption (cf Fig.1a).

Our comparison with Tsuchiya et al.’s numerical model would be fair apart from one theoretical concern. The progenitor in their best simulation is a two-component ”nucleated” model with a rigid nucleus modeled by a extended-particle of  $10^7 M_\odot$  with a half mass radius of 35pc on top of a live satellite of  $0.8 \times 10^{10} M_\odot$  with a Hernquist profile of half-mass radius 1.4kpc; the dynamical friction of the Hernquist halo helps to deliver the nucleus eventually to an orbit similar to that of  $\omega$ -Centauri . However, a closer examination reveals a subtle inconsistency in making the nucleus rigid: the tidal force from the Hernquist halo beats the self-gravity of this fluffy nucleus at its half-mass radius by a factor of a few, so it could not have stayed and being moved as one piece. Nevertheless, one could have used a more contact, hence more plausible model of the rigid nucleus, say, with a total mass of  $3 \times 10^6 M_\odot$  and a smaller half-mass radius of 7pc, which are closer to the observed mass and half-mass radius of  $\omega$ -Centauri . With this in mind, the formal inconsistency in Tsuchiya et al.’s best simulation seems to be harmless, and their model shows that  $\omega$ -Centauri could in principle be the remnant of a massive satellite on an orbit of initial apo-to-peri ratio of (about) 60kpc/2kpc.

## 6. Summary

We have used a set of simple analytical models of dynamical friction and tidal massloss to explore the orbital decay for a dwarf satellite with a range of initial specific angular momentum and massloss history. These models greatly simplifies the orbital dynamics and tidal interaction of satellites without losing the accuracies of more rigourous and sophisticated numerical simulations. We follow the evolution of satellites in the mass-distance plane, and find generally very little evolution of specific angular momentum by dynamical friction. The progenitors of inner halo globular clusters and substructures can not be born on orbits of

comparable angular momentum as present-day halo satellite galaxies. The central cores of observed dwarfs are also not dense enough to survive the tides within 15 kpc. Any BHs in these satellites may also be difficult to reach and merger with the supermassive BH in the host galaxy. In general, satellite remnants (BHs, globulars and streams) tend to hang up in the outer halo.

I thank Ken Freeman, George Meylan, Jim Pringle, Floor van Leeuwen for enlightening discussions during the  $\omega$ -Centauri conference at IoA, and Oleg Gnedin, Mike Irwin, Pavel Kroupa, Mark Wilkinson for a careful reading of an earlier draft. I thank Vladimir Korchagin, Dana Dinescu & Toshio Tsuchiya for patiently explaining their paper to me, James Binney and Kenji Bekki for answering queries of their models. This work is made possible by a special grant of research time from my 1-year-old MianMian and YiYi.

## REFERENCES

- Bekki K. & Freeman K.C. 2003, MNRAS, 346, L11 (astro-ph/0310348)
- Binney J.J., & Tremaine S., 1987, ‘Galactic Dynamics’ (Princeton Univ. Press),
- Blais-Ouellette, S., Carignan, C., Amram, P., & Côté, S. 1999, AJ, 118, 2123
- Carignan, C., & Purton, C. 1998, ApJ, 506, 125
- ChandraSekhar S. 1943, ApJ, 97, 255
- Dekel A., Devor J, Hetzroni G, 2003, MNRAS, 341, 326
- Dinescu, D. I., Girard, T. M., and van Altena, W. F. 1999, AJ, 117, 1792
- Fellhauer M. & Kroupa P. 2002, MNRAS, 330, 642
- Ferguson A., Irwin, M., Ibata R., Lewis G., Tavar N. 2002, AJ, 124, 1452
- Freeman, K. C. 1993, in the globular cluster-galaxy connection, ed. Graeme H. Smith and Jean P. Brodie, ASP Conf. 48, p608
- Gnedin, O.Y., Zhao, H., Pringle, J.E., Fall, S.M., Livio, M., & Meylan, G. 2002, ApJ, 568, L23
- Harris, W. E. 1996, AJ, 112, 1487
- Ibata R., Gilmore G, Irwin M. 1994, Nature, 370, 194

- Ibata, R. A., Wyse, R. F. G., Gilmore, G., Irwin, M. J., & Suntzeff, N. B. 1997, *AJ*, 113, 634
- Jiang I., & Binney J. 2000, *MNRAS*, 314, 468
- Johnston, K.V., Zhao,H., Spergel D.N., Hernquist L. 1999, *ApJ*, 512, 109
- Kendall P., Magorrian J., Pringle J., 2003, *MNRAS*, 346, 1078
- Klypin, A., Zhao, H.S., Somerville, R. 2002, *ApJ*, 573, 597
- Kroupa P. & Bastian U. 1997, *NewA*, 2, 77
- Larsen S.S. 2001, *AJ*, 122, 1782
- Lynden-Bell D. & Lynden-Bell R.M. 1995, *MNRAS*, 275, 429
- Martin N.F., Ibata R., et al. 2004, *MNRAS*, 348, 12 (astro-ph/0311010)
- McConnachie A.W., Irwin, M., Ibata R., Ferguson A. , Lewis G., Tavis N. 2003, *MNRAS*, 343, 1335
- McMillan S.L.W. & Portegies-Zwart S.F. 2003, *ApJ*, 596, 314
- Meylan, G., Sarajedini, A., Jablonka, P., Djorgovski, S. G., Bridges, T., & Rich, R. M. 2001, *AJ*, 122, 830
- Mizutani, A., Chiba, M., & Sakamoto, T. 2003, *ApJ*, 589, L89
- Mouri H. & Taniguchi Y. 2003, *ApJ*, 585, 250
- Mulder, W.A. 1983, *A&A*, 117, 9
- Newberg H.J. et al. 2003, 596, 191 (astro-ph/0309162)
- Piatek S. et al. 2002, *AJ*, 124, 3198
- Penarrubia J., Kroupa P. & Boily, C. 2002, *MNRAS*, 333, 779
- Rich, R. M., Mighell, K. J., Freedman, W. L., & Neill, J. D. 1996, *AJ*, 111, 768
- Schweizer A.E., Cudworth K., & Majewski S. 1997, *ASP Conf. Ser.* 127, *Proper Motions and Galactic Astronomy*, ed. R.M. Humphreys (San Francisco, ASP), 132
- Sellwood, J. 2000, *ApJ*, 540, L1

Syer D., White S. 1998, MNRAS, 293, 337

Tsuchiya, T., Dinescu, D. I., Korchagin, V. I., 2003, ApJL, 589, 29

Tsuchiya, T., Korchagin, V. I., Dinescu, D. I., 2004, MNRAS, in press (astro-ph/0402410)

Wright L. 2003, PhD thesis, Cambridge University.

Zhao, H. S. 2002, in ASP Conf. Ser. 265, Omega Centauri: A Unique Window into Astrophysics, ed. F. van Leeuwen, J. D. Hughes, & G. Piotto (San Francisco: ASP), 391

Zhao, H. S. 1998, ApJ, 500, L149

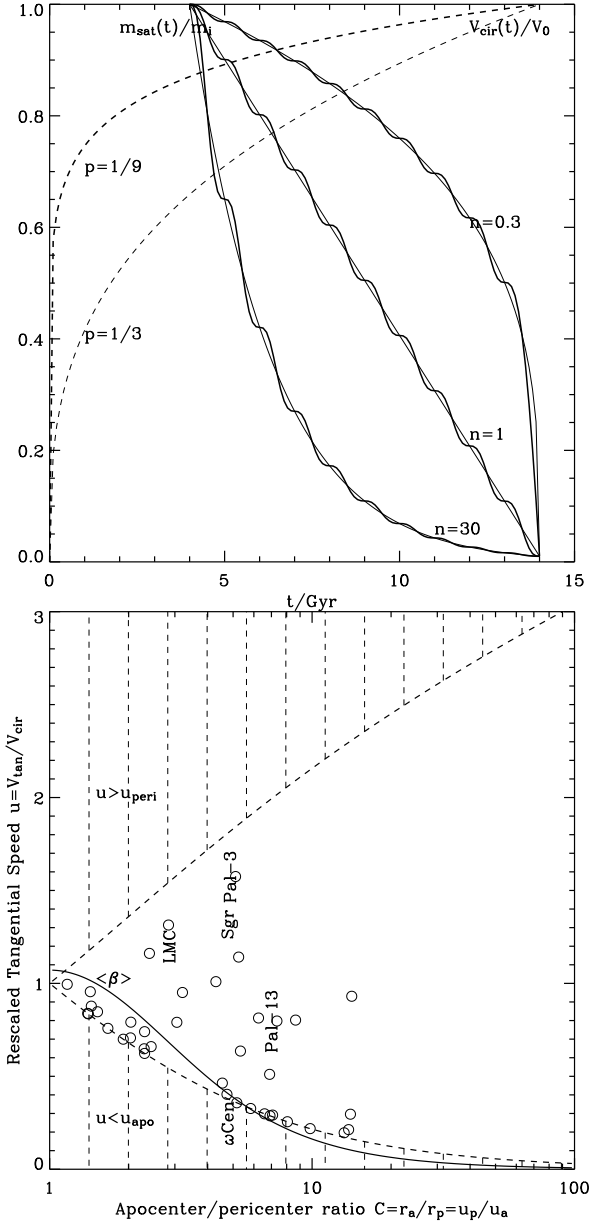


Fig. 1.— Panel (a) shows the rescaled satellite mass  $m(t)/m_i$  (thick solid) and effective mass  $\mu(t)/\mu_i$  (thin solid) as a function of time for three models (marked by their  $n$ -values), and the rescaled host halo rotation speed  $V_{\text{cir}}(t)/V_0$  for the past Hubble time for two models (marked by their  $p$ -values). Panel (b) shows the boundaries of the rescaled tangential speed  $\frac{V_a}{V_{\text{cir}}} \leq u \leq \frac{V_p}{V_{\text{cir}}}$ , (lower and upper dashed lines) as functions of the apo-to-peri ratio  $C = \frac{r_a}{r_p} = \frac{V_p}{V_a}$ . Also shown is the mean effective mass conversion factor  $\langle \beta \rangle = \frac{\mu}{m}$  (solid line, cf. eq. 21), normalized to  $\ln \Lambda = 2.5$ . Note that the value of  $\langle \beta \rangle$  varies *only* a factor of two among the Milky Way satellites and globular clusters (circles); the pile-up of some clusters along the apocenter line is due to distance errors (data taken from Dinescu et al. 1999 and references therein).

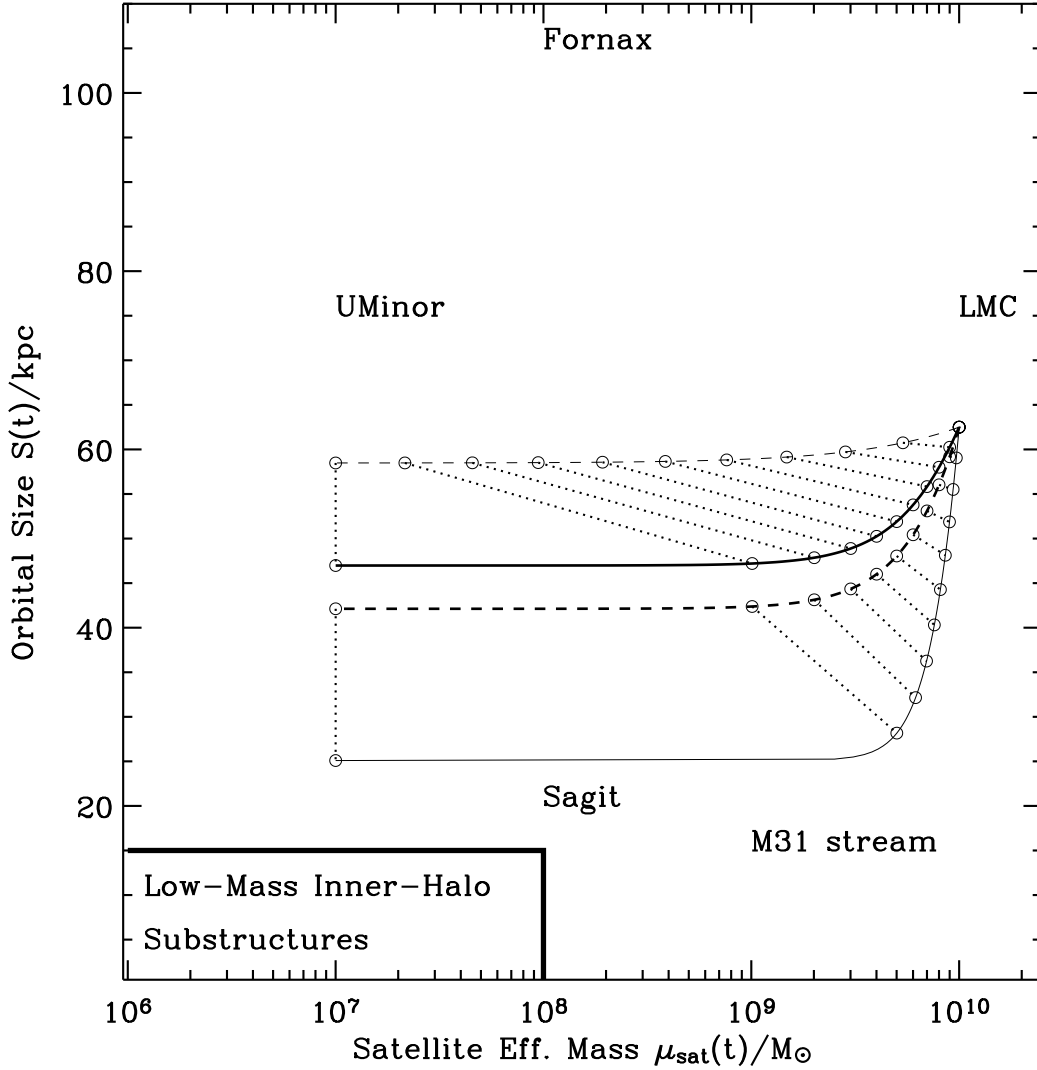


Fig. 2.— shows the predicted evolution histories of a satellite in the plane of its effective mass  $\mu(t)$  vs. characteristic orbital size  $S(t) \equiv \frac{j(t)}{200 \text{ km s}^{-1}}$ . The hatched horn-like areas show models with moderate potential growth ( $p = \frac{1}{3}$ , **upper horn**) with a massloss between exponential ( $n = \infty$ , upper dashed boundary) and linear ( $n = 1$ , lower solid boundary), and models with static potential ( $p = 0$ , **lower horn**) with a massloss between linear ( $n = 1$ , upper dashed boundary) and accelerated ( $n = 0.3$ , lower solid boundary). A massive satellite starts at  $t_i = 4$  Gyrs from the upper right corner with an effective mass  $\mu(t_i) = \langle \beta \rangle_i m_i = 10^{10} M_\odot$  with angular momentum  $j_i = 250 \text{ km s}^{-1} \times 50 \text{ kpc}$ , and ends with an effective mass of  $10^7 M_\odot$ . For different assumptions of the massloss rate, the intermediate mass and position of the remnant are indicated with a time step of 1 Gyr. Note the failure to deliver remnants to the lower left corner. Also indicated are the estimated orbital size and the mass of the satellite galaxies of the Milky Way and M31.



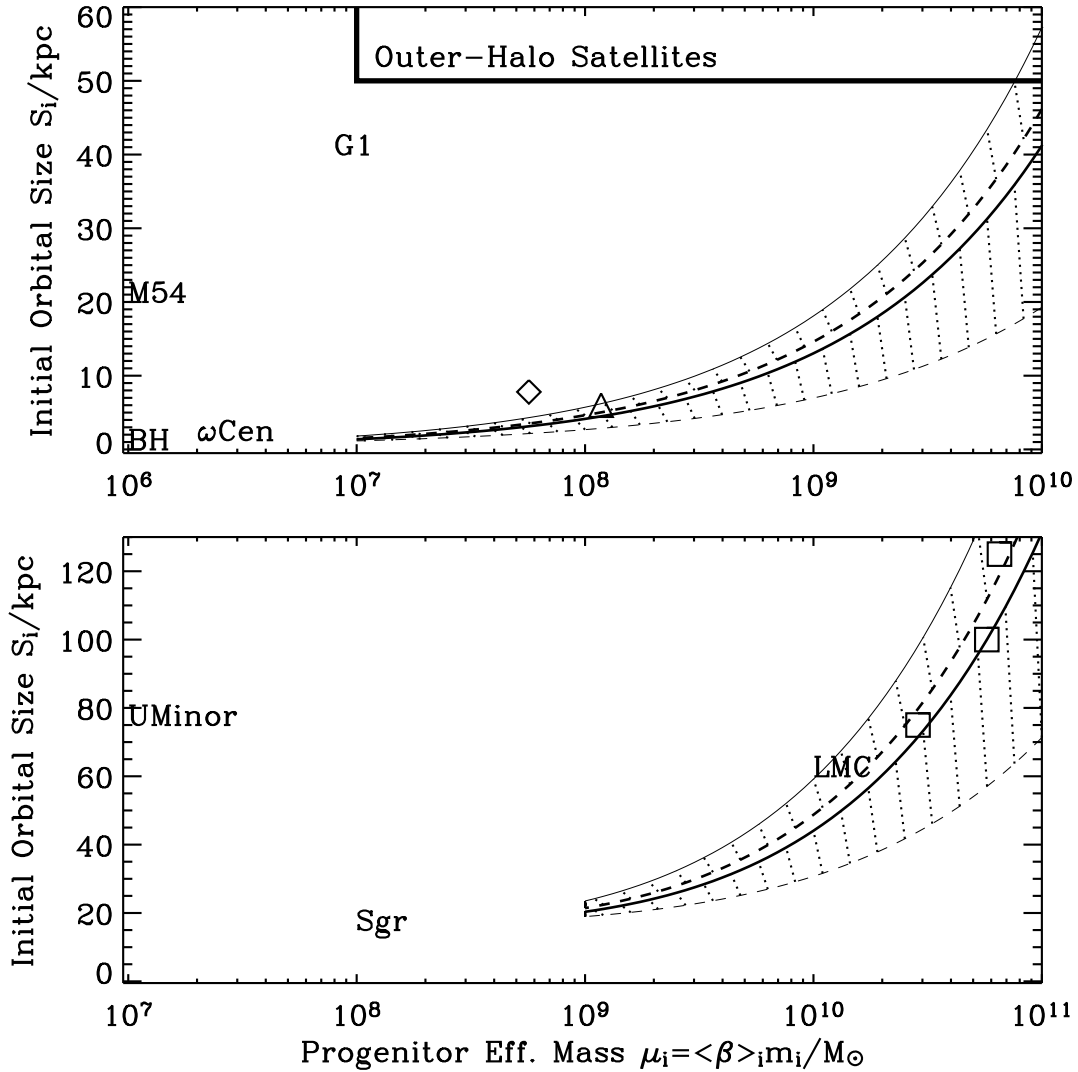


Fig. 3.— shows initial conditions to deliver a  $\omega$ -Centauri-like  $10^6 M_\odot$  remnant to the Galactic center (upper panel) or deliver a Sgr-like remnant of  $10^8 M_\odot$  to the inner galaxy (lower panel). Dynamical friction works too slow for an object initially to the upper left of the shaded regions in the plane of the initial effective mass of the progenitor  $\mu_i$  vs. the initial orbital size  $S_i = j_i/200$ . Different line types and shaded regions have the same meaning as in Figure 2 (thick dashed line for a linear massloss in a static potential). The symbols are simulations of Bekki & Freeman (diamond) and Tsuchiya et al. (triangle) for the  $\omega$ -Centauri, and Jiang & Binney (squares for their Models A, F, K) for the Sgr; we assume the same Colomb logarithm  $\ln \Lambda = 2.5$  for both our model and these simulations. Also indicated are the present values for the several satellites of the Milky Way and M31 and a central million solar mass BH.

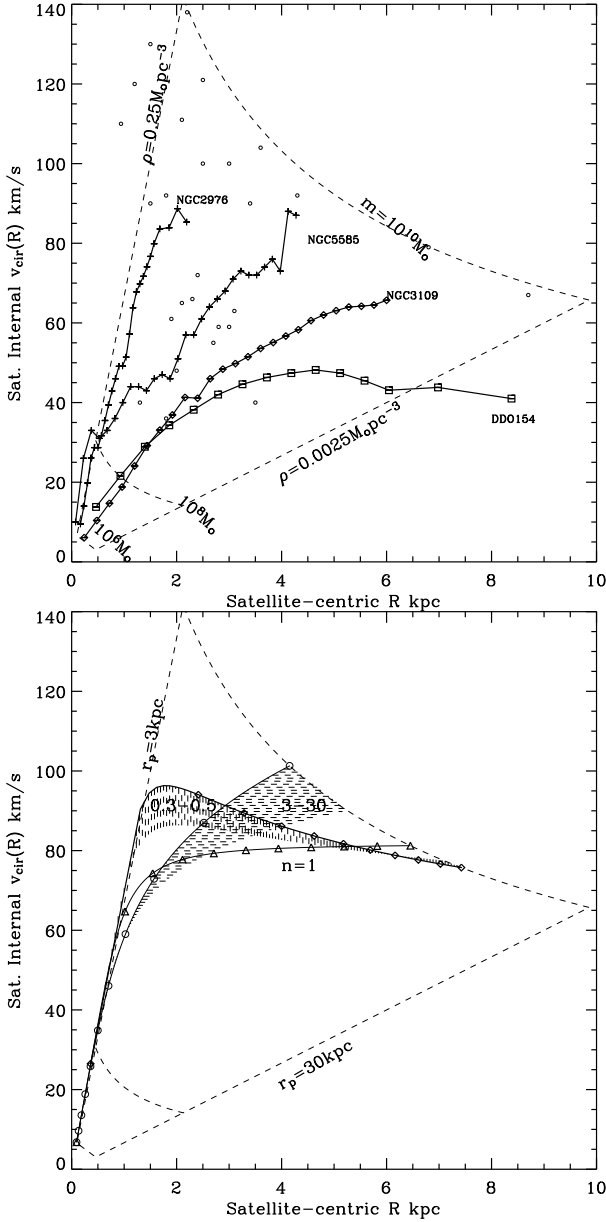


Fig. 4.— **(panel a)** shows the rotation curves of four observed dwarf galaxies (as labelled), and the core radius vs. maximum rotation velocity for another two dozen dwarf galaxies (small circles). Also shown is a region bounded by solid body rotation curves of a uniform volume density  $\rho_t = 0.25 M_\odot \text{pc}^{-3}$  or  $0.0025 M_\odot \text{pc}^{-3}$  (two thin dashed lines from left to right), and Keplerian rotation curves of a point mass of  $10^{10} M_\odot$ ,  $10^8 M_\odot$ , or  $10^6 M_\odot$  (three thin dashed curves from top to bottom). **(panel b)** shows the inferred circular velocity curves of a  $10^{10} M_\odot$  progenitor for different assumed massloss index  $n$ ; it is inferred so that a remnant of  $10^6 M_\odot$  is placed on an orbit with an apo-to-peri ratio of about 15 kpc : 3 kpc. Symbols indicate the tidal radii at look-back time 1, 2, ..., 10 Gyr for the  $n = 0.3$  model (diamond),  $n = 1$  model (triangles), and  $n = 30$  model (circles). Hatched regions are for  $n = 0.3 - 0.5$  and  $n = 3 - 30$ .

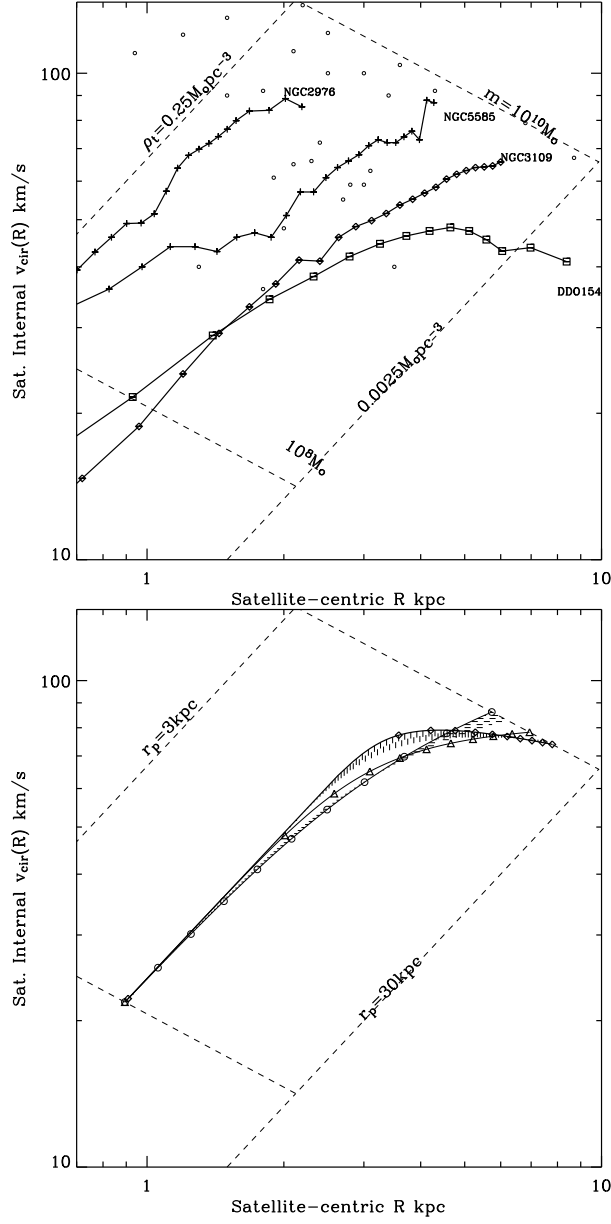


Fig. 5.— Similar to previous figure, except in logarithmic scale, and for (**panel b**) we assume the remnant is  $10^8 M_{\odot}$  on an orbit with  $r_a : r_p = 40 \text{ kpc} : 8 \text{ kpc}$ .

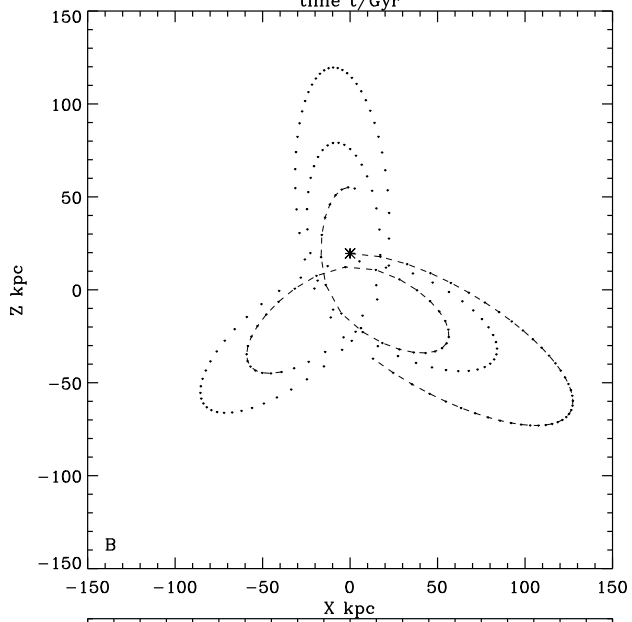
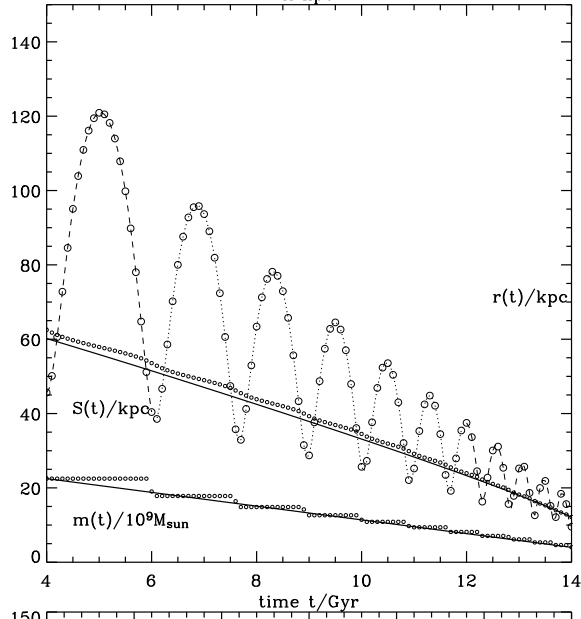
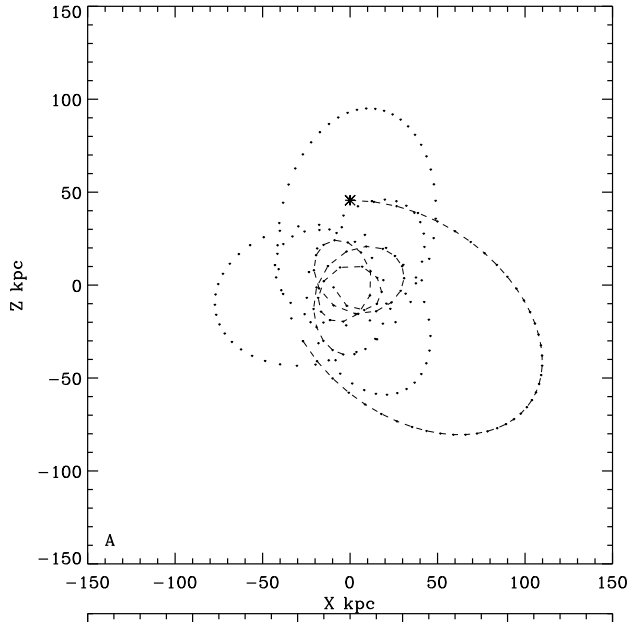


Table 1. Orbital size of known satellites of the Local Group

Object	Spec. Ang. Mom.	Orbital size	Ref
	$j_0 = \mathbf{r} \text{kpc} \times \mathbf{v} \text{ km s}^{-1}$	$S_0 \equiv \frac{j_0}{200} \text{kpc}$	
$\omega$ -Centauri	$5 \text{kpc} \times 50 \text{ km s}^{-1}$	1.25	(1)
Sgr stream	$16 \text{kpc} \times 260 \text{ km s}^{-1}$	20.8	(2)
Magellanic stream	$60 \text{kpc} \times 250 \text{ km s}^{-1}$	75	(3)
Ursa Minor	$70 \text{kpc} \times 200 \text{ km s}^{-1}$	70	(4)
Fornax	$138 \text{kpc} \times 310 \text{ km s}^{-1}$	213	(5)
M31 stream	$150 \text{kpc} \times 20 \text{ km s}^{-1}$	15	(6)
Canis Major dSph	$15 \text{kpc} \times 200 \text{ km s}^{-1}$	15	(7)

References. — (1) Dinescu et al. 1999; (2) Ibata et al. 1997; (3) Kroupa & Bastian 1997; (4) Schweizer et al. 1997 ; (5) Piatek et al. 2002; (6) McConnachie et al. 2003; (7) Martin et al. 2004.

